Quasi-two-dimensional transfer of elastic waves

Nicolas P. Trégourès and Bart A. van Tiggelen
Laboratoire de Physique et Modélisation des Milieux Condensés, CNRS/Université Joseph Fourier, Boîte Postale 166, 38042 Grenoble Cedex 09, France

(Received 3 April 2001; revised manuscript received 13 March 2002; published 3 September 2002)

A theory for multiple scattering of elastic waves is presented in a heterogeneous plate bounded by two flat free surfaces, whose horizontal size is infinite and whose transverse size is smaller than the mean free path of the waves. We derive a time-dependent, quasi-two-dimensional radiative transfer equation (i.e., two horizontal dimensions with a finite number of vertical mode) that describes the coupling of the eigenmodes of the layer (surface Rayleigh waves, shear horizontal waves, and Lamb waves). The fundamentally different element is that the traction-free boundary conditions are treated on the level of the wave equation, whereas at the same time elastic transfer can be considered over macroscopic horizontal distances. Expressions are found that relate the small-scale fluctuations to the lifetime of the modes and to their mode-coupling rates. We discuss the diffusion approximation that simplifies the mathematics of this model significantly, and which should apply at large lapse times. Finally, this model facilitates a study of coherent backscattering near the plate surface for different sources and for different detection configurations.

DOI: 10.1103/PhysRevE.66.036601 PACS number(s): 46.40.Cd, 91.30.Dk, 62.30.+d

I. INTRODUCTION

Multiple scattering of waves in random media has been studied throughout the previous century [1] and is still an active domain of research [2,3]. The subject is rich in its interdisciplinarity aspects, with roots in astrophysics, optics, acoustics, and quantum mechanics, with many fundamental problems, among which wave localization, the random laser, speckles, enhanced backscattering [4], optics of liquid crystals [5,6], and (broken) time-reversal symmetry [7] are some contemporary examples. In addition, such studies have found potential applications, like in polymer dispersed liquid crystals, in remote sensing, in (medical) imaging, and in seismology.

A general theory for multiple scattering is very complex. The reason is that it depends heavily on geometry and dimensionality, as well as on the nature of the waves. Different studies of multiple scattering consider different geometries in which the scattering occurs, and for which some sort of specific mathematical simplification facilitates a solution. In the quasi-one-dimensional (quasi-1D) geometry only the lowest radial diffusion mode of a tube is excited, and is therefore very useful for rigorous mesoscopic studies of transmission fluctuations (see contributions in Ref. [8]). The ''slab geometry,'' with ''infinite'' transverse width is the convenient geometry employed to model optical laboratory experiments, even in complex situations [5]. Media with higher symmetry are also regularly found. One-dimensional disordered systems are popular for their theoretical rigor [9]. Two-dimensional random media are encountered in studies of the quantum Hall effect, plasmons, bending waves [10], and microwaves [11], or in acoustics [12]. In seismology, a (quasi) 2D picture might apply to the scattering of guided waves in the crust [13].

The present work introduces the so-called quasi-2D approximation. We will show that this approximation applies to radiative transfer in a geometry whose vertical size is smaller than the mean free path. It provides a radiative transfer equation for modes, rather than for specific intensities. Many properties of this equation will be addressed in detail for elastic waves. A fundamentally different feature in this model is that the vertical direction is treated on the microscopic level of the wave equations, and not on the macroscopic level of the transport equations. The latter usually provide knowledge on scales comparable to and beyond the mean free path [1]. Their compatibility with the underlying wave equations is therefore regularly questioned, notably in the so-called mesoscopic regime where interference effects seem to persist. In addition, several experiments require knowledge on length scales of the order of the wavelength, particularly in the case of surface detection, where the boundary conditions have to be coped with on the level of the wave equation. This, is for instance, true for the observation of seismic wave propagation in the crust, Refs. [14–17], or in the elastic coherent backscattering experiments by de Rosny, Tourin, and Fink [18] in silicon wafers. In ultrasonics, the conventional equation of elastic radiative transfer has been studied in great detail [19–22]. The quasi-2D approximation facilitates a study of many contemporary mesoscopic phenomena, such as equipartition and coherent backscattering, with the explicit consideration of the free surface.

The setup of this paper is as follows. In Sec. II we look at the wave equation for elastic waves, and we will define the Green's function for elastic wave propagation. In Sec. III we introduce small-scale fluctuations and define the ensemble-averaged Green's function. This provides us with the extinction times of all elastic modes. They will serve to define our quasi-2D approximation. In Sec. IV, the transport equation is derived, which describes the time evolution of the ensemble-averaged energy contents of all individual modes, and whose stationary solution exhibits equipartition of energy between all modes. In Sec. V, we discuss the application of the diffusion approximation to this quasi-2D model, introducing a $N \times N$ diffusion tensor for N modes. Finally, in Sec. VI we investigate coherent backscattering using our quasi-2D approximation for different source and detection configurations. Section VII is devoted to conclusions and perspectives.

II. A SCHRÖDINGER-TYPE EQUATION FOR ELASTIC WAVES

In this section we will formulate the mathematics of elastic wave propagation in a way that is suited to apply conventional methods in multiple scattering of waves. Many elements have already been discussed very thoroughly by Ryzhik *et al.* [23], and some will be recalled here for convenience [24]. We start with Newton's second law for the elastic displacement $\mathbf{u}$ at time t and position $\mathbf{r}$,

$$\rho(\mathbf{r})\partial_t^2\mathbf{u}_i=\partial_j\sigma_{ij}(\mathbf{r})+\mathbf{f}_i(\mathbf{r},t). \tag{1}$$

Here, $\rho(\mathbf{r})$ is the local mass density, $\mathbf{f}(\mathbf{r},t)$ is an external force per unit volume, and $\sigma_{ij}(\mathbf{r})$ is the stress tensor which, by Hooke's law, is given by [14,15,25]

$$\sigma_{ij}(\mathbf{r})=C_{ijkl}(\mathbf{r})\varepsilon_{kl}(\mathbf{r})=\lambda(\mathbf{r})\varepsilon_{kk}(\mathbf{r})\delta_{ij}+2\mu(\mathbf{r})\varepsilon_{ij}(\mathbf{r}), \tag{2}$$

with $\varepsilon_{kl}=\frac{1}{2}(\partial_k u_l+\partial_l u_k)$ the strain tensor. As always, summation over repeated indices is assumed implicitly. The second equality applies to an isotropic elastic medium, in which case the fourth-rank tensor C_{ijkl} can only have two independent contributions, proportional to the Lamé moduli $\lambda(\mathbf{r})$ and $\mu(\mathbf{r})$. Inserting the expression (2) of the stress tensor in Eq. (1) provides the wave equation for the elastic displacement $\mathbf{u}$,

$$\begin{aligned}\rho(\mathbf{r})\partial_t^2u_i-[\lambda(\mathbf{r})+\mu(\mathbf{r})]\partial_i\partial_k u_k-\mu(\mathbf{r})\partial_i\partial_i u_i\\ =[\partial_i\lambda(\mathbf{r})](\partial_k u_k)+2[\partial_j\mu(\mathbf{r})]\varepsilon_{ji}+\mathbf{f}_i(\mathbf{r},t).\end{aligned} \tag{3}$$

If the Lamé coefficients $\lambda(\mathbf{r})$ and $\mu(\mathbf{r})$ are independent of $\mathbf{r}$, Eq. (3) further simplifies to the well-known wave equation

$$\partial_t^2\mathbf{u}-\frac{\lambda+2\mu}{\rho(\mathbf{r})}\boldsymbol{\nabla}\boldsymbol{\nabla}\cdot\mathbf{u}+\frac{\mu}{\rho(\mathbf{r})}\boldsymbol{\nabla}\times\boldsymbol{\nabla}\times\mathbf{u}=\frac{\mathbf{f}_i(\mathbf{r},t)}{\rho(\mathbf{r})}, \tag{4}$$

where the second term of the left-hand side of Eq. (4) corresponds to a compressional bulk wave (also called P wave) which propagates with the velocity $v_p=\sqrt{\lambda+2\mu/\rho(\mathbf{r})}$ and the third term of the left-hand side of Eq. (4) describes a shear bulk wave (S wave) with velocity $v_s=\sqrt{\mu/\rho(\mathbf{r})}$. For reasons that will become clear in the following sections, we will not use the form (3) of the elastic wave equation but formulate an equivalent equation more suitable for the purpose of elastic wave scattering and transport.

The total energy of the elastic displacement $\mathbf{u}$ is given by [25]

$$E_{\mathrm{tot}}=\int d^3\mathbf{r}[\tfrac{1}{2}\rho(\mathbf{r})(\partial_t\mathbf{u})^2+\tfrac{1}{2}\lambda(\mathbf{r})(\boldsymbol{\nabla}\cdot\mathbf{u})^2+\mu(\mathbf{r})\varepsilon_{ij}^*\varepsilon_{ji}]. \tag{5}$$

It is customary to split off a term $\mu(\mathrm{curl}\,\mathbf{u})^2$ (describing pure shear wave energy) and $2\mu(\mathrm{div}\,\mathbf{u})^2$ (contributing to compressional energy) from the last term, leaving a rest term I,

$$\begin{aligned}E_{\mathrm{tot}}=\int d^3\mathbf{r}[\tfrac{1}{2}\rho(\mathbf{r})(\partial_t\mathbf{u})^2+\tfrac{1}{2}(\lambda(\mathbf{r})\\ +2\mu(\mathbf{r}))(\boldsymbol{\nabla}\cdot\mathbf{u})^2+\tfrac{1}{2}\mu(\mathbf{r})(\mathrm{curl}\,\mathbf{u})^2+I].\end{aligned} \tag{6}$$

This identifies four terms as "kinetic energy," "compressional energy," "shear energy," and an interference term I [17,25,26]. The latter vanishes for plane waves with either pure transverse or pure longitudinal polarization. Following Ryzhik *et al.* [23] we shall now introduce the vector field,

$$\boldsymbol{\Psi}(\mathbf{r},t)=\begin{pmatrix}\sqrt{\frac{\lambda(\mathbf{r})}{2}}\mathbf{p}\cdot\mathbf{u}\\ \sqrt{\frac{\rho(\mathbf{r})}{2}}i\partial_t u_i\\ -i\sqrt{\mu(\mathbf{r})}\varepsilon_{ij}\end{pmatrix}, \tag{7}$$

where we have defined the operator $\mathbf{p}=-i\boldsymbol{\nabla}$. This vector has 13 components among which only 9 are independent since ε_{ij} is a symmetric tensor whose trace is proportional to the first component, $\sqrt{(\lambda/2)}\mathbf{p}\cdot\mathbf{u}$, of $\boldsymbol{\Psi}$. The physical interpretation of the vector field $\boldsymbol{\Psi}$ is made clear by introducing the Cartesian scalar product

$$\langle\boldsymbol{\Psi}(t)|\boldsymbol{\Psi}(t)\rangle\equiv\int d^3\mathbf{r}\boldsymbol{\Psi}(\mathbf{r},t)^*\cdot\boldsymbol{\Psi}(\mathbf{r},t)=E_{\mathrm{tot}}, \tag{8}$$

i.e., the total elastic energy (5). As a result, $\boldsymbol{\Psi}$ can be regarded as a *complex amplitude for elastic energy*. The first and third components of $\boldsymbol{\Psi}$ correspond to the *potential* energy amplitude while the second component describes the *kinetic* energy amplitude. Moreover, it can readily be checked that the wave equation (3) is equivalent to the following Schrödinger-type equation for $\boldsymbol{\Psi}$ [23]:

$$i\partial_t|\boldsymbol{\Psi}(\mathbf{r},t)\rangle=\mathbf{K}(\mathbf{r},\mathbf{p})\cdot|\boldsymbol{\Psi}(t)\rangle+|\boldsymbol{\Psi}_f(t)\rangle, \tag{9}$$

with the time-evolution operator

$$\mathbf{K}=\begin{pmatrix}0 & \sqrt{\lambda(\mathbf{r})}(\vec{\mathbf{p}})\frac{1}{\sqrt{\rho(\mathbf{r})}} & \vec{\vec{\mathbf{0}}}\\ \frac{1}{\sqrt{\rho(\mathbf{r})}}\mathbf{p}\downarrow\sqrt{\lambda(\mathbf{r})} & \vec{\mathbf{0}}\downarrow & \frac{1}{\sqrt{\rho(\mathbf{r})}}\vec{\vec{\mathbf{L}}}(\mathbf{p})\downarrow\sqrt{2\mu(\mathbf{r})}\\ \mathbf{0}\downarrow\downarrow & \sqrt{2\mu(\mathbf{r})}\vec{\mathbf{L}}(\mathbf{p})\downarrow\downarrow\frac{1}{\sqrt{\rho(\mathbf{r})}} & \vec{\vec{\mathbf{0}}}\downarrow\downarrow\end{pmatrix} \tag{10}$$

and the external force term $\mathbf{\Psi}_f(\mathbf{r},t)\equiv[\mathbf{0},-\mathbf{f}(\mathbf{r},t)/\sqrt{\rho(\mathbf{r})},\vec{\vec{\mathbf{0}}}]$. We have introduced the third rank tensor $L_{ijk}(\mathbf{p})\equiv\frac{1}{2}(\mathbf{p}_i\delta_{jk}+\mathbf{p}_j\delta_{ik})$ and used the formal Dirac notation for vector fields to facilitate later the more convenient mode base. The number of arrows determines the order of the tensor. For clarity, we have put horizontal arrows when they contract in a right-hand side product with a vector. If $\lambda(\mathbf{r})$ and $\mu(\mathbf{r})$ are real valued, the matrix $\mathbf{K}$ is manifestly symmetrical with respect to the ordinary Cartesian scalar product (8).

Equation (9) can easily be Laplace transformed ($\mathrm{Im}z>0$). This yields the solution

$$|\mathbf{\Psi}(\mathbf{z})\rangle=[z-\mathbf{K}]^{-1}[i|\mathbf{\Psi}(t=0)\rangle+|\mathbf{\Psi}_f(\mathbf{z})\rangle]. \qquad (11)$$

The operator $[z-\mathbf{K}]^{-1}\equiv\mathbf{G}(\mathbf{z})$ will be called the Green's function, and is introduced here for future need. It is convenient to define $t=0$ just before the source sets in so that $\mathbf{\Psi}(t=0)=0$ and the force field becomes the source for wave propagation.

We would like to point out that the description of elastic waves in terms of the vector field $\mathbf{\Psi}$ and its time-evolution equation (9) is mathematically equivalent to the wave equation (3) even when the mass density and the Lamé coefficients depend on $\mathbf{r}$. The formulation (9) is more convenient to study elastic wave scattering and transport.

III. PROPAGATION OF ELASTIC WAVES IN A LAYER

We consider a heterogeneous elastic plate of infinite horizontal dimension and of thickness H. In this paper, we will assume that both sides of the plate are free surfaces and we therefore neglect any leakage of energy out of the plate. Leaking of energy is an additional complex problem that will be considered in future work. The present model incorporates coherent reflection, mode conversions, and, most importantly, surface Rayleigh waves at the surfaces of the plate.

The disorder in the plate will be modeled by random fluctuations of the mass density $\rho(\mathbf{r})$, and the Lamé coefficients $\lambda(\mathbf{r})$ and $\mu(\mathbf{r})$. The explicit statistics of the fluctuations will be specified more precisely later on. Fluctuations of the order of only a few percent shall be treated as first order perturbations.

A. Elastic eigenmodes of a homogeneous plate

The displacement eigenmodes of a homogeneous elastic plate have been discussed in great detail by Weaver [27,28]. They can be separated into two subclasses, each of these classes consists of an infinite number of branches. Moreover, due to the symmetry of the boundary conditions of the plate, all subclasses consist of symmetric and antisymmetric branches. The simplest class is the one of shear horizontal (SH) modes. These waves are pure shear waves with a displacement field polarization parallel to the boundaries and normal to the direction of propagation [27,28]. The class of Lamb modes consists of a mixture of shear and compressional displacements since a pure compressional displacement does not obey the traction-free boundary conditions.

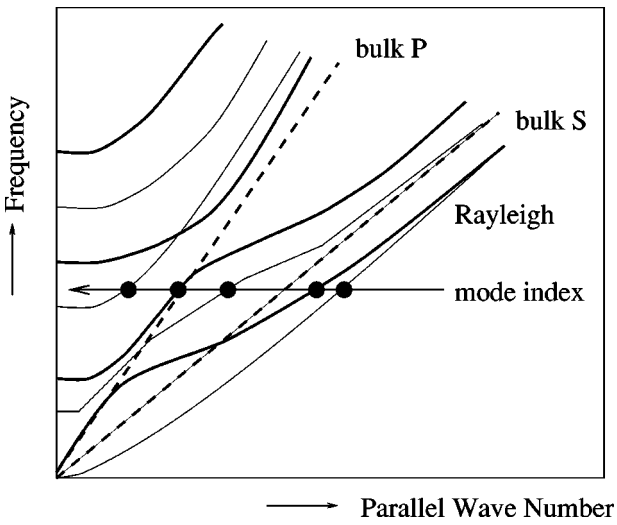

FIG. 1. Schematic plot of the dispersion law of the elastic Rayleigh-Lamb eigenmodes in a layer bounded by two free surfaces. Bold lines indicate symmetric branches, straight lines indicate antisymmetric modes. Only modes of different symmetry are allowed to cross. The two dashed lines indicate the pure shear or pure compressional excitations. The surface Rayleigh waves propagate somewhat slower than pure S waves. For an actual calculation of the dispersion laws we refer to Fig. 2 of Weaver [27].

Figure 1 gives a schematic plot of the dispersion law of Lamb modes. The representation (7) of each mode can be obtained straightforwardly from its displacement and we shall denote it by $\mathbf{\Psi}_n$. The index n is a discrete index that labels, at constant frequency (Fig. 1), the symmetric and antisymmetric Lamb modes and symmetric and antisymmetric SH modes in the plate.

Let us discuss the Lamb modes at a given frequency, indicated by the horizontal line in Fig. 1, in the direction of the arrow. The two dashed lines indicate purely shear and purely compressional waves. The first two antisymmetric modes (first two black dots on the right) are the symmetric and antisymmetric Rayleigh surface modes, respectively. Their displacement is evanescent for both the compressional and the shear component. Rayleigh modes propagate somewhat slower than bulk S or P waves. As a result they lie on the right side of the dashed lines. The third antisymmetric Lamb mode (third black dot) lies between the dashed lines. This mode is evanescent for its compressional component but has a shear displacement that is close to bulk behavior. It behaves like a pure shear mode as we go away from either one of the free surfaces. As a result, its total potential energy is mostly due to shear excitation. Finally, the mode at the very left in Fig. 1 lies on the left of both dashed lines. Even deep inside the plate this mode is a mixture of P and S displacements. As we increase the frequency, the number of modes increases but the organization of Lamb modes sketched above stays essentially intact. One always encounters two surface Rayleigh modes (one symmetric and one antisymmetric), modes that are evanescent in P but not in S and modes that are both bulk S and bulk P.

By translational symmetry, the eigenmodes can be chosen proportional to transverse plane waves with wave number $\mathbf{k}$. We will treat them initially as $\exp(i\mathbf{k}\cdot\mathbf{x})/\sqrt{A}$, with a discrete

contribution of $\mathbf{k}$ to the label n as a result of the periodic boundary conditions on both sides of a square plate with surface A, and eventually take the limit $A\to\infty$.

B. Extinction time of the eigenmodes Ψ_n

We will now assume the presence of disorder in the plate. As a result, each eigenmode $\mathbf{\Psi}_n$ of the homogeneous plate will achieve a finite lifetime τ_n.

The first step to formulate a transport theory is to calculate the Green's function averaged over this random disorder [29]. Let the disorder be represented by a perturbation $\delta\mathbf{K}$ in the time-evolution operator: $\mathbf{K}=\mathbf{K}_0+\delta\mathbf{K}$. The ensemble-averaged ''retarded'' (outgoing) Green's function at frequency ω is given by

$$\langle \mathbf{G}(\mathbf{z}=\omega+i0)\rangle=\left\langle \frac{1}{\omega+i0-\mathbf{K}}\right\rangle \equiv \frac{1}{\omega+i0-\mathbf{K}_0-\mathbf{\Sigma}(\omega)}. \tag{12}$$

This ''Dyson'' equation defines the mass operator $\mathbf{\Sigma}(\omega)$. The lowest order contribution is given by [30]

$$\mathbf{\Sigma}(\omega)=\left\langle \delta\mathbf{K}\cdot\frac{1}{\omega+i0-\mathbf{K}_0}\cdot\delta\mathbf{K}\right\rangle + O(\delta\mathbf{K})^3. \tag{13}$$

Next, we can insert the complete and orthonormal set $\{\mathbf{\Psi}_n\}$ of the homogeneous plate, defined above. Standard first-order perturbation theory yields

$$\mathbf{G}(\omega)=\sum_n \frac{|\mathbf{\Psi}_n\rangle\langle\mathbf{\Psi}_n|}{\omega-\omega_n-\Sigma_n(\omega)}, \tag{14}$$

with

$$\Sigma_n(\omega)=\sum_m \langle|\langle\mathbf{\Psi}_n|\delta\mathbf{K}|\mathbf{\Psi}_m\rangle|^2\rangle\frac{1}{\omega-\omega_m+i0}. \tag{15}$$

The imaginary part of this parameter is negative, and identified with $-1/2\tau_n$, where τ_n is the extinction time of mode n.

In general, $\rho(\mathbf{r})$, $\lambda(\mathbf{r})$, and $\mu(\mathbf{r})$ are correlated random variables. The general case is very complex, since not only the fluctuations themselves come in but, by Eq. (10), also their spatial derivatives. A number of special cases can be treated exactly, such as the case of fluctuations in density, with constant elastic coefficients λ and μ. Another simplification happens when we consider only fluctuations in the two Lamé coefficients $\lambda(\mathbf{r})$ and $\mu(\mathbf{r})$, and keep ρ constant. This case is richer physically and far more interesting since it still allows a separate control over the extinction and scattering of S and P waves. If we assume that $\rho(\mathbf{r})=\rho_0$, $\lambda(\mathbf{r})=\lambda_0+\delta\lambda(\mathbf{r})$ and $\mu(\mathbf{r})=\mu_0+\delta\mu(\mathbf{r})$, with λ_0 and μ_0 the coefficients of the homogeneous layer, we find

$$\delta\mathbf{K}=\frac{1}{\sqrt{\rho_0}}\begin{pmatrix} 0 & [\delta\lambda(\mathbf{r})/2\sqrt{\lambda_0}]\vec{\mathbf{p}} & \vec{\vec{\mathbf{0}}} \\ \mathbf{p}\downarrow[\delta\lambda(\mathbf{r})/2\sqrt{\lambda_0}] & \vec{\mathbf{0}}\downarrow & \vec{\vec{\mathbf{L}}}(\mathbf{p})\downarrow[\delta\mu(\mathbf{r})/2\sqrt{2\mu_0}] \\ \mathbf{0}\downarrow\downarrow & [\delta\mu(\mathbf{r})/2\sqrt{2\mu_0}]\vec{\mathbf{L}}(\mathbf{p})\downarrow\downarrow & \vec{\vec{\mathbf{0}}}\downarrow\downarrow \end{pmatrix}. \tag{16}$$

A straightforward calculation, employing integration by parts, finally leads to

$$\begin{aligned}\langle|\langle\mathbf{\Psi}_n|\delta\mathbf{K}|\mathbf{\Psi}_m\rangle|^2\rangle=\omega^2\int d^3\mathbf{r}\int d^3\mathbf{r}'\{&\langle\delta\lambda(\mathbf{r})\delta\lambda(\mathbf{r}')\rangle\\ &\times(\nabla\cdot\mathbf{u}_n)^*(\nabla\cdot\mathbf{u}_m)(\nabla'\cdot\mathbf{u}_n')^*(\nabla'\cdot\mathbf{u}_m')\\ &+\delta\mu(\mathbf{r})\delta\mu(\mathbf{r}')\rangle\mathrm{Tr}\,\varepsilon_n^*\cdot\varepsilon_m\mathrm{Tr}(\varepsilon_n')^*\cdot\varepsilon_m'\\ &+\langle\delta\lambda(\mathbf{r})\delta\mu(\mathbf{r}')\rangle\\ &\times(\nabla\cdot\mathbf{u}_n)^*(\nabla\cdot\mathbf{u}_m)\mathrm{Tr}(\varepsilon_n')^*\cdot\varepsilon_m'+\mathrm{c.c.}\}.\end{aligned} \tag{17}$$

To evaluate $\Sigma_n(\omega)$ we must specify the spatial correlations between the Lamé coefficients. The simplest choice is to assume correlations that are short range with respect to the wavelength,

$$\langle\delta\lambda(\mathbf{r})\delta\lambda(\mathbf{r}')\rangle=\sigma_\lambda^2(z)\delta(\mathbf{r}-\mathbf{r}'), \tag{18a}$$

$$\langle\delta\mu(\mathbf{r})\delta\mu(\mathbf{r}')\rangle=\sigma_\mu^2(z)\delta(\mathbf{r}-\mathbf{r}'), \tag{18b}$$

$$\langle\delta\mu(\mathbf{r})\delta\lambda(\mathbf{r}')\rangle=\sigma_{\mu\lambda}^2(z)\delta(\mathbf{r}-\mathbf{r}'). \tag{18c}$$

Without extra difficulty, we can still allow for a depth dependence of the correlation functions. The present approach can also be used for the more realistic case of ''Rayleigh-Gans'' scatterers, in which case the fluctuations are still small, but with long correlation length [31]. Σ_n can be evaluated for a big plate for which $\Sigma_m\to\Sigma_i A\int d^2\mathbf{k}/(2\pi)^2$, including a sum over the different branches. All factors A cancel if a transverse plane wave normalization $\exp(i\mathbf{k}\cdot\mathbf{x})$ is adopted. For the extinction time of mode branch j at frequency ω, we find

$$\frac{1}{\tau_j(\omega)}=\omega^2\sum_i n_i\int\frac{d^2\hat{\mathbf{k}}_i}{2\pi}W(i\mathbf{k}_i,j\mathbf{k}_j), \tag{19}$$

with $n_i(\omega)\equiv k_i(\omega)/v_i(\omega)$ in terms of the group velocity $\mathbf{v}_i=d\omega_i/d\mathbf{k}_i$. The ''mode scattering cross section'' is defined as

$$W(i\mathbf{k}_i, j\mathbf{k}_j) = \int_0^H dz \{\sigma_\lambda^2(z) |\nabla \cdot \mathbf{u}_{i\mathbf{k}_i}|^2 |\nabla \cdot \mathbf{u}_{j\mathbf{k}_j}|^2 + \sigma_\mu^2(z) |\mathrm{Tr}\, \varepsilon^*_{i\mathbf{k}_i} \cdot \varepsilon_{j\mathbf{k}_j}|^2 + 2\sigma^2_{\mu\lambda}(z) \times \mathrm{Re}(\nabla \cdot \mathbf{u}^*_{i\mathbf{k}_i} \cdot \nabla \cdot \mathbf{u}_{j\mathbf{k}_j} \mathrm{Tr}\, \varepsilon^*_{i\mathbf{k}_i} \cdot \varepsilon_{j\mathbf{k}_j})\}. \quad (20)$$

We have chosen to split off the factor n_i, so that this matrix is symmetric. According to our model the extinction time τ_j does not depend on the direction of the horizontal wave number $\mathbf{k}_j$.

The *imaginary* part of the ensemble-averaged Green's function is directly related to the excitations of the waves [32]. The spectral density $\mathcal{N}(\omega)$ per unit surface can be expressed as

$$\mathcal{N}(\omega) = -\frac{1}{\pi A} \mathrm{Tr}\, \mathrm{Im}\, \mathbf{G}(\omega) = \frac{1}{\pi} \sum_i \int \frac{d^2\mathbf{k}}{(2\pi)^2} \frac{1/2\tau_{i\mathbf{k}}}{[\omega - \omega_{i\mathbf{k}}]^2 + 1/4\tau^2_{i\mathbf{k}}}. \quad (21)$$

Due to scattering, all modes are spectrally broadened. The separation in wave number of two adjacent modes with the same frequency (see Fig. 1) is typically of order $1/H$. The uncertainty in k is typically $1/v_{i\mathbf{k}}\tau_{i\mathbf{k}}$, with $v_{i\mathbf{k}}$ the group velocity of the mode. If

$$\tau_{i\mathbf{k}} > H/v_{i\mathbf{k}}, \quad (22)$$

one can assume that different modes at fixed $\mathbf{k}$ do not overlap, except at a few degeneration points where the dispersion curves for modes with different symmetry (i.e., SH and Lamb) cross. This assumption is the *quasi-two-dimensional approximation* (Q2DA). In the Q2DA we find for the spectral density per unit surface $\mathcal{N}(\omega) = (2\pi)^{-1} \Sigma_i n_i$, showing that n_i, defined in Eq. (19), represents the spectral weight per unit surface of mode i at frequency ω in phase space.

In the following, all time scales will be normalized to the mean free time of S waves in an infinite medium with the same amount of disorder. This time depends only on σ_μ^2 that can be related to the correlation length and the shear velocity fluctuations. Figure 2 shows extinction times for different modes index, calculated from Eqs. (19) and (20), normalized to the mean free time of S waves in an infinite medium. The plate thickness is $H = 20.2\lambda_S$, for which $N = 106$ guided modes exist. The disorder is chosen uniform in the whole plate, and the spatial correlations among the Lamé coefficients is taken equal: $\sigma_\lambda^2 = \sigma_\mu^2 = \sigma^2_{\mu\lambda}$. SH modes show an extinction time very similar to the extinction time of S waves in an infinite medium τ_s^∞. On the other hand, the Lamb modes present a more complex pattern. Rayleigh modes clearly show a shorter extinction time, Lamb modes with an evanescent compressional component behave very much like a bulk S wave. Finally, Lamb modes with both bulk compressional and bulk shear components behave in a complicated fashion but tend to have an extinction time larger than S waves in an infinite medium. They are not sensitive to the compressional fluctuations in the bulk and therefore live longer.

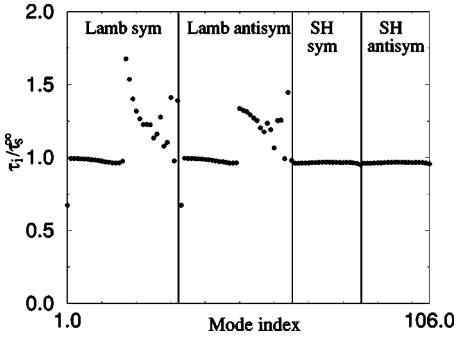

FIG. 2. Extinction times τ_i for the different modes i as a result of elastic scattering, calculated from Eq. (19). The extinction times are normalized to the mean free time τ_S^∞ of S waves in a 3D infinite random medium. The disorder is chosen to be uniform in the whole plate and the spatial correlation between the Lamé coefficients is chosen equal. The plate thickness is $H = 20.2\lambda_s$, having $N = 106$ modes. The two Rayleigh waves have $\tau_i \approx 0.7\tau_S^\infty$. The modes with relatively high τ_i have a significant P component throughout the layer.

In the case of dominant μ fluctuations, $\sigma_\lambda^2 \ll \sigma_\mu^2$ (dominant fluctuations in shear velocity) the Lamb modes with both "bulk" compressional and "bulk" shear components will achieve a larger extinction time. When the λ fluctuations dominate, $\sigma_\lambda^2 \gg \sigma_\mu^2$ (strong compressional velocity fluctuations), the same Lamb modes with "bulk" compressional and shear displacements will have an even shorter extinction time.

We would like to emphasize that the lifetime of Rayleigh waves is not well described by our model since they suffer most from surface disorder (fluctuations in height), which was not included in Eqs. (18). This might be done in future work.

IV. ELASTIC TRANSPORT EQUATION FOR THE PLATE

The next task is the formulation of an elastic transport equation in the quasi-2D approximation. Basic observable is the ensemble-averaged intensity Green's function $\langle \mathbf{G}(\omega^-) \times \mathbf{G}(\omega^+)^* \rangle$, with $\omega^\pm = \omega \pm \frac{1}{2}\Omega$. It can be expressed in the complete base $\{\mathbf{\Psi}_n\}$ of the homogeneous plate, giving rise to the matrix element $L(\omega, \Omega)_{nn'mm'}$. The Bethe-Salpeter equation [29,32] for this object reads

$$\mathcal{L}_{nn'mm'}(\omega, \Omega) = G_n(\omega^+) G_{n'}(\omega^-)^* \left[\delta_{nm}\delta_{n'm'} + \sum_{ll'} U_{nn'll'}(\omega, \Omega) \mathcal{L}_{ll'mm'}(\omega, \Omega) \right], \quad (23)$$

with G_n the Dyson Green's function defined in Eq. (12), and a new object U called the irreducible vertex. Upon introduc-

ing $\Delta G_{nn'}(\omega,\Omega) \equiv G_n(\omega^+) - G_{n'}^*(\omega^-)$ (idem for $\Delta\Sigma$) this equation can be rearranged into

$$[\Omega + (\omega_n - \omega_{n'}^*) - \Delta\Sigma_{nn'}]\mathcal{L}_{nn'mm'}(\omega,\Omega) = \Delta G_{nn'}(\omega,\Omega)\left[\delta_{nm}\delta_{n'm'} + \sum_{ll'} U_{nn'll'} \times (\omega,\Omega)\mathcal{L}_{ll'mm'}(\omega,\Omega)\right]. \quad (24)$$

This equation is still exact. We will now carry through a number of approximations relevant to our problem. For small disorder, the vertex U is given by [30]

$$U_{nn'll'}(\omega,\Omega) = \langle\langle \boldsymbol{\Psi}_n | \delta\mathbf{K} | \boldsymbol{\Psi}_l\rangle\langle \boldsymbol{\Psi}_{n'} | \delta\mathbf{K} | \boldsymbol{\Psi}_{l'}\rangle\rangle. \quad (25)$$

For short-range correlations, as specified in Eqs. (18), the vertex U can be straightforwardly related to the cross section $W(i\mathbf{k}_i, j\mathbf{k}_j)$ defined in Eq. (20). For typical wave packets $\Omega \ll \omega$ (i.e., a wave packet contains many cycles) so that we can neglect Ω in any functional dependence on frequency ("slowly varying envelope approximation"). The index n consists of one discrete branch index j, and one index $\mathbf{k}$ that becomes continuous as $A \to \infty$. The Q2DA neglects all overlaps between different branches, so that $\Delta G(\omega,\Omega)_{nn'} \to 2\pi i \delta_{jj'}\delta[\omega - \omega_j(\mathbf{k})]$. If we let $\mathbf{k} - \mathbf{k}' = \mathbf{q}$, and $S_m(\omega)$ the source in mode representation, a new observable quantity $L_{j\mathbf{k}}$ can be defined as

$$\sum_{mm'} \mathcal{L}_{nn'mm'}(\omega,\Omega) S_m S_{m'}^* \equiv 2\pi\delta[\omega - \omega_{j\mathbf{k}}]\delta_{jj'} \times L_{j\mathbf{k}}(\mathbf{q},\Omega). \quad (26)$$

In space-time the Q2D transport equation reads

$$\left[\partial_t + \mathbf{v}_j \cdot \boldsymbol{\nabla} + \frac{1}{\tau_{j\mathbf{k}_j}}\right] L_{j\mathbf{k}}(\mathbf{x},t) = |S_{j\mathbf{k}}(\omega)|^2 \delta(t)\delta(\mathbf{x}) + \omega^2 \sum_{j'} \int \frac{d^2\hat{\mathbf{k}}_{j'}}{2\pi} \times n_{j'} W(j\mathbf{k}_j, j'\mathbf{k}_{j'}) L_{j'\mathbf{k}_{j'}}(\mathbf{x},t). \quad (27)$$

We will use this equation as a starting point for our calculations. The equation is essentially two-dimensional, with a finite number of modes (of order $2H\omega/\beta$) to take care of the third, vertical dimension. The great advantage of this equation is that the boundary conditions of the elastic waves have been dealt with *exactly*, i.e., on the level of the wave equation, contrary to conventional transport equations [21,22,33]. We see that $L_{j\mathbf{k}}(\mathbf{x}, t)$ can be interpreted as the *specific intensity* of the mode $(j\mathbf{k}_j)$ at frequency ω, at horizontal position $\mathbf{x}$, at a time t after the release of energy by the source. The source term $S_{j\mathbf{k}}(\omega)$ is given by

$$S_{j\mathbf{k}}(\omega) = \langle \boldsymbol{\Psi}_{j\mathbf{k}} | \boldsymbol{\Psi}_f \rangle = \omega \int d^3\mathbf{r} \cdot \mathbf{f}^*(\mathbf{r},\omega) \cdot \mathbf{u}_{j\mathbf{k}}(\mathbf{r}). \quad (28)$$

Since $\mathbf{u}_{j\mathbf{k}}$ is an eigenfunction for which the energy (5) has been normalized, we see that $|S_{j\mathbf{k}}|^2$ has the dimension of energy. Since $(\Omega, \mathbf{q})$ dependence has been neglected in the source, it emerges in our transport equation as a $\delta(t)\delta(\mathbf{x})$ in space-time.

A. Equipartitioned solution

Equation (27) has one very important property that has been discussed in great detail in the literature. By recalling expression (19) for the extinction time, it follows immediately that the specific intensity with the property that its total mode energy $\int d^2\mathbf{x} L_{j\mathbf{k}_j}(\mathbf{x},\mathbf{t})$ is independent of the mode index j and independent of the horizontal direction of propagation $\mathbf{k}$, is a stationary solution for $t > 0$ of the transport equation. All solutions converge to this solution regardless of the nature and position of the source. This implies that finally all modes have an equal share in the *total* energy contents of the plate. This phenomenon is called *equipartition* [17,33–36], and is believed to be a fundamental feature of the solution of transport equations at large lapse times, provided absorption is absent, or at least small [37]. According to our definition (26), the total spectral energy per unit surface in the regime of equipartition is given by

$$E_\omega(t) = \sum_j \int \frac{d^2\mathbf{k}}{(2\pi)^2} \int d^2\mathbf{x}\, L_{j\mathbf{k}}(\mathbf{x},t) 2\pi\delta(\omega - \omega_{j\mathbf{k}}) \to \text{const} \sum_j n_j. \quad (29)$$

The equipartitioned solution can be used to evaluate different energy ratios, such as S/P, or kinetic to potential energy ratio, as a function of depth [17]. At $z = 0$ these values agree with a calculation done by Weaver for a *semi-infinite* random medium [35], and were recently observed with seismic waves in Mexico [17].

B. Dynamics of the equipartition process

We will now introduce the spectral energy density $E_i(\mathbf{x},t)$ of mode i per unit surface, and its current density $\mathbf{J}_i(\mathbf{x},t)$ according to

$$E_i(\mathbf{x},t) \equiv \int \frac{d^2\mathbf{k}}{(2\pi)^2} 2\pi\delta(\omega - \omega_{i\mathbf{k}}) L_{i\mathbf{k}}(\mathbf{x},t) = n_i \int \frac{d^2\hat{\mathbf{k}}}{2\pi} L_{i\mathbf{k}_i}(\mathbf{x},t), \quad (30a)$$

$$\mathbf{J}_i(\mathbf{x},t) \equiv \int \frac{d^2\mathbf{k}}{(2\pi)^2} 2\pi\delta(\omega - \omega_{i\mathbf{k}}) \mathbf{v}_i L_{i\mathbf{k}}(\mathbf{x},t) = n_i \int \frac{\mathrm{d}^2\hat{\mathbf{k}}}{2\pi} \mathbf{v}_i L_{i\mathbf{k}_i}(\mathbf{x},t). \quad (30b)$$

An exact equation of continuity can be found from Eq. (27) by integrating over $\mathbf{k}_i$,

$$\partial_t E_i(\mathbf{x},t) + \boldsymbol{\nabla}\cdot\mathbf{J}_i(\mathbf{x},t) = \left[n_i \int \frac{d^2\hat{\mathbf{k}}}{2\pi} \left| S_{i\mathbf{k}_i}(\omega) \right|^2 \right] \delta(\mathbf{x})\,\delta(t) - \sum_j C_{ij} E_j(\mathbf{x},t), \tag{31}$$

with the ''mode-conversion matrix,''

$$C_{ij} = \frac{\delta_{ij}}{\tau_i} - \omega^2 n_i \int \frac{d^2\hat{\mathbf{k}}_j}{2\pi} W(i\mathbf{k}_i, j\mathbf{k}_j). \tag{32}$$

The mode-conversion matrix C has an eigenvalue 0 with eigenvector $\{n_i\}$, associated with the equipartition. Its $N-1$ nonzero eigenvalues, whose eigenvectors can be called ''Stokes parameters'' since they characterize the polarization of the mode, determine the dynamics of the equipartition process. The solution of Eq. (31) depends on the initial conditions, i.e., how the initial release of energy was distributed among the different modes, as described by $S_{i\mathbf{k}}(\omega)$.

Figure 3 shows all eigenvalues of the matrix C in the case of a plate of thickness $H = 20.2\lambda_S$, for which the number of modes is $N = 106$. The disorder has been assumed uniform in the whole plate and the spatial correlation among all Lamé coefficients is chosen equal: $\sigma_\lambda^2 = \sigma_\mu^2 = \sigma_{\mu\lambda}^2$. The time scale has been normalized to the mean free time of S waves in an infinite medium, with the same amount of disorder, i.e., as described by Eqs. (18).

The largest eigenvalue (associated with the shortest lifetime) has an eigenvector made up of the symmetric and antisymmetric Rayleigh modes. This statement, however, is sensitive to the distribution of the heterogeneity in the plate. If the plate would not have any disorder within a wavelength from the two free surfaces, the Rayleigh modes would not suffer much from the disorder, so that their lifetime would have been very large. When the disorder would have been localized close to the free surface, the Rayleigh modes would have ended up with a relatively short lifetime. The eigenvectors associated with the flat plateau in Fig. 3 consist of modes whose shear component strongly dominates over the compressional part. As a result, their lifetimes are very similar to the shear mean free time of an S wave in an infinite medium. The last set of eigenvectors, with substantially smaller lifetimes than the rest, have a strong compressional component. They were already associated with longer lifetimes in Fig. 2.

For dominant μ fluctuations, $\sigma_\lambda^2 \ll \sigma_\mu^2$, the picture does not change drastically since the Lamb modes are always dominated by shear. Only for dominant λ fluctuations, $\sigma_\lambda^2 \gg \sigma_\mu^2$, the structure of eigenmodes of the mode-conversion matrix C is modified considerably. Eigenvalues that were previously associated with ''bulk'' P and S vectors now have their lifetime much shorter.

Figure 4 shows, for different kind of sources, how the initial release of energy is distributed among the different

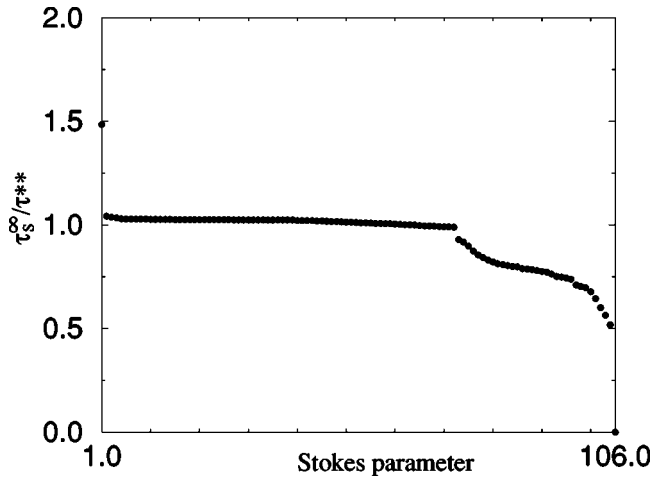

FIG. 3. Eigenvalues $1/\tau^{**}$ of the collision matrix C, defined in Eq. (32), for a plate thickness $H = 20.2\lambda_s$ with 106 modes. They are normalized to the inverse mean free time $1/\tau_S^\infty$ of S waves in an infinite medium. The disorder is uniform in the whole plate and the spatial correlation between all Lamé coefficients is equal. Mode 1 is dominated by surface waves and decays rapidly; mode 106 is the equipartitioned mode with infinite lifetime. The flat plateau has modes with dominating shear displacements.

modes. Figure 4(a) shows an isotropic explosion at a depth $\lambda_s/3$ from the free surface. An explosion is a purely compressional source, and does not excite any SH modes. Among the Lamb modes it excites preferentially the modes that are ''bulk'' for both compressional and shear components as well as Rayleigh modes. A source at a larger depth will no longer directly excite the Rayleigh modes since they have a penetration length of the order of the wavelength.

Figure 4(b) applies for a double couple in the x-y plane at a depth $\lambda_s/3$ from the free surface. Contrary to the isotropic explosion, a double couple in the x-y plane strongly excites the SH modes. Since the source is close to the free surface Rayleigh modes are excited as well. The Lamb modes which are ''bulk'' for the shear component but only evanescent for the compressional component are also excited.

Figures 4(c) and 4(d) show the mode distribution for a double couple in the plane x-z for two different depths of the source, $\lambda_s/3$ and $5\lambda_s$. When the source is located close to the free surface the majority of the energy is released among the Rayleigh modes. Two Rayleigh modes are out of scale in Fig. 4(c) but carry in fact half of the released energy. When the source is situated deep in the plate the pattern becomes very rich. One can see that the Rayleigh modes are no longer excited.

V. DIFFUSION APPROXIMATION

Despite the many simplifications that have been carried out, the final transport equation (27) is still difficult to solve numerically. In future work, we intend to adapt our Monte-Carlo simulations, developed to solve the 3D radiative transfer equation [16], to this modified equation. In this section we shall carry out a final and rather familiar simplification that facilitates a numerical solution.

The diffusion approximation is typically valid at large lapse times, when currents start to become small. In that case, the specific intensity of mode i can be written as

$$L_{i\mathbf{k}}(\mathbf{q},\Omega)=\frac{1}{n_i}\left[E_i(\mathbf{q},\Omega)+\frac{2}{v_i^2}\mathbf{v}_i\cdot\mathbf{J}_i(\mathbf{q},\Omega)+\cdots\right], \quad (33)$$

with $n_i=k_i/v_i$ the density of mode i in phase space introduced earlier. In real space $\mathbf{q}$ transforms into the 2D gradient $\boldsymbol{\nabla}$. Inserting the series (33) into Eq. (27) leads to the relation

$$\mathbf{J}_i(\mathbf{x},t)=-\sum_j D_{ij}\boldsymbol{\nabla}E_j(\mathbf{x},t). \quad (34)$$

This relation is recognized as a generalized Fick's Law [38], generalized, because it involves different individual modes at the cost of one dimension. The *diffusion matrix* is given by

$$(\mathbf{D}^{-1})_{ij}=2\left(\frac{\delta_{ij}}{v_i^2\tau_i}-\frac{\omega^2}{n_j}\int\frac{d^2\hat{\mathbf{k}}_j}{2\pi}W(i\mathbf{k}_i,i\mathbf{k}_j)\frac{\mathbf{v}_i\cdot\mathbf{v}_j}{v_i^2v_j^2}\right). \quad (35)$$

It is easy to check the following relation:

$$\frac{D_{ij}}{D_{ji}}=\frac{n_i}{n_j}. \quad (36)$$

Combining Eqs. (34) and (31) and transforming back to space-time yields the generalized 2D diffusion equation,

$$\partial_t E_i(\mathbf{x},t)-\sum_j D_{ij}(\omega)\triangle E_j(\mathbf{x},t)$$

$$=S_i(\omega)\delta(\mathbf{x})\delta(t)-\sum_j C_{ij}(\omega)E_j(\mathbf{x},t), \quad (37)$$

where

$$S_i(\omega)=n_i\int\frac{d^2\hat{\mathbf{k}}}{2\pi}|S_{i\mathbf{k}}(\omega)|^2. \quad (38)$$

This diffusion equation is an ordinary partial differential equation that can be solved by conventional means. For an infinite plate no boundary conditions have to be specified: the boundary conditions at the two free surfaces have been taken care of exactly. For this reason, the Q2D diffusion approximation is not expected to break down near the boundaries, as was noticed by Turner and Weaver for the conventional diffusion approximation [22].

Equation (37) still captures the time evolution of the different elastic modes of the plate, and can thus be used to

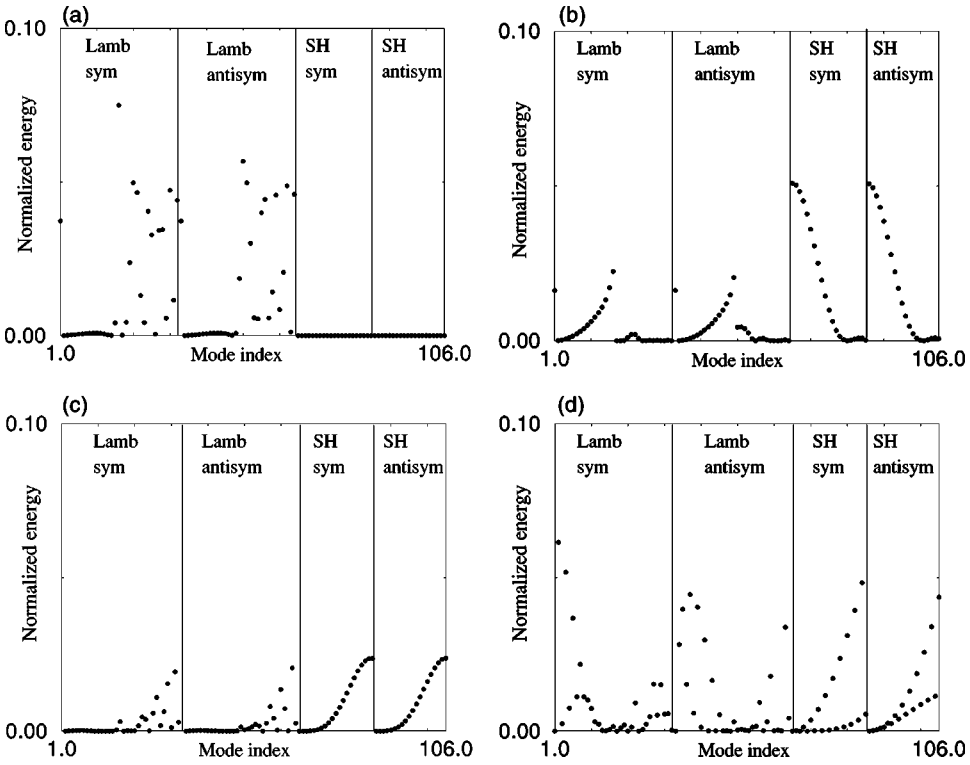

FIG. 4. Initial energy distribution among the different modes, for different sources. The plate thickness is $H=20.2\lambda_s$ with 106 modes. (a) Isotropic explosion source at a depth $\lambda_s/3$ from the free surface. No SH waves are excited. The only waves that are excited are the two surface waves, and the Lamb waves with a nonevanescent P component. (b) Double-couple source in the x-y plane at a depth $\lambda_s/3$ from the free surface. In this case all modes are excited with a dominance of SH waves and Lamb waves with an evanescent P component. (c) Double-couple source in the x-z plane at a depth $\lambda_s/3$ from the free surface. With respect to (b), we infer that the excitation of Lamb waves with a nonevanescent P is suppressed. The two Rayleigh modes, however, are out of scale and carry half of the released energy. (d) Double-couple source in the x-z plane as in (c), now at a depth $5\lambda_s$ from the free surface. The Rayleigh waves are no longer directly excited, but all other modes are excited.

study polarization properties. Integrating Eq. (37) over the horizontal coordinate **r** gives for the time evolution of the total modal energy

$$\partial_t E_i(t) = S_i(\omega)\,\delta(t) - \sum_j C_{ij}(\omega) E_j(t). \qquad (39)$$

In fact, this equation follows directly from Eq. (31) without the need to apply the diffusion approximation. Its formal solution is $E_i(t) = \Sigma_j [\exp(-\mathbf{C}t)]_{ij} S_j(\omega)\,\theta(t)$. This can easily be evaluated using the complete set of eigenmodes of C, calculated earlier.

Figure 5(a) shows the time evolution of the energy among the different modes for an isotropic explosion at a depth $\lambda_s/3$ from the free surface. The initial modal energy distribution was already shown in Fig. 4(a). For the sake of clarity we only display the evolution of three subclasses of modes (Rayleigh, Lamb, SH) and not the whole distribution. Rayleigh modes are excited but not SH modes since the source is purely compressional. With the passage of time, the mode occupation changes as a result of the dynamics of the equipartition process and finally tends to the equipartitioned distribution which does not depend on nature and location of the source.

Figure 5(b) shows the time evolution of two ''observable'' energy ratios measured at the free surface: the ratio of shear to compressional potential energy, E_s/E_p, and the one of the horizontal to vertical kinetic energy H^2/V^2. After a few shear wave mean free times, the energy ratios stabilize at their predicted equipartition value $E_s/E_P = 7.19$, $H^2/V^2 = 1.77$ [17]. The ratios E_s/E_p and H^2/V^2 increase monotonically which is due to the compressional nature of the source.

Figures 5(c) and 5(d) present the equipartition process for a double-couple source deep in the plate ($5\lambda_s$ from the free surface). For such a source the Rayleigh modes are not excited while the other Lamb modes and SH modes are strongly excited [recall Fig. 4(d)]. The initial ratio of shear to compressional energy at the free surface is higher than the one for the explosion source due to the shear nature of the source. However, in both cases the energy distributions converge towards an equipartitioned distribution which is independent of the nature of the source and its location. Note that for an explosion the equipartition process takes a much longer time, typically $6\,\tau_s^\infty$. For the double-couple source in Figs. 5(c) and 5(d) it is typically equal to τ_s^∞.

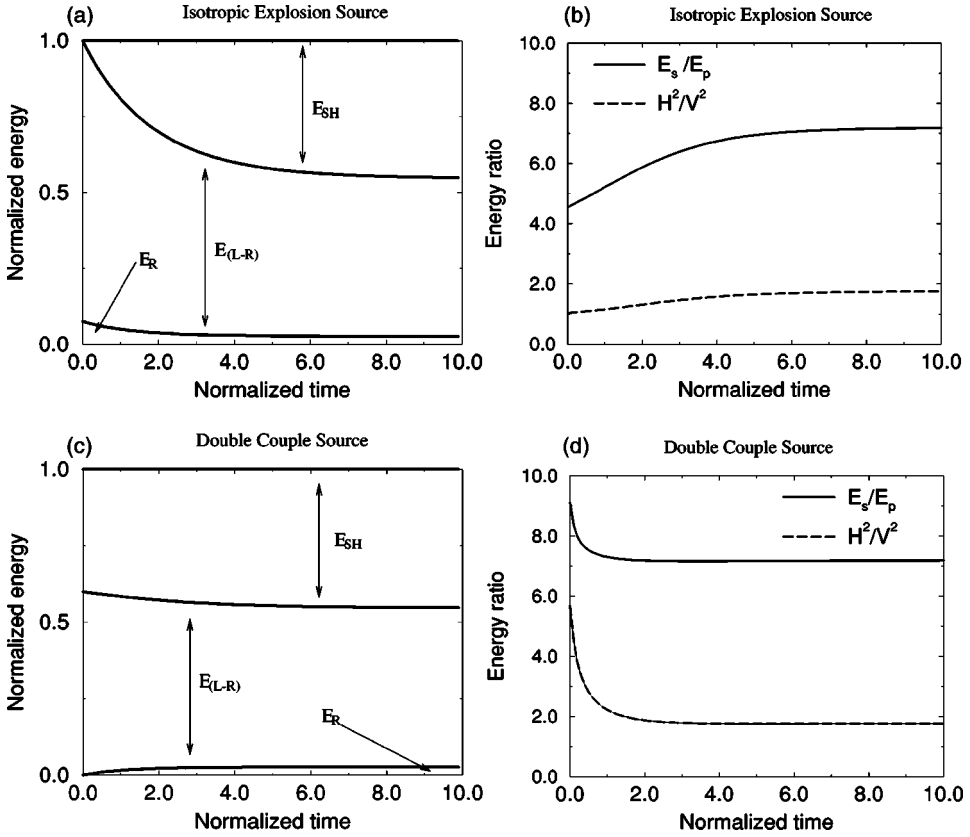

FIG. 5. Dynamics of the energy distribution among the various modes, as predicted by the diffusion equation (39) and for two different sources. The double arrows in the two figures on the left indicate the total amount of energy contained in either SH waves, Lamb waves, or Rayleigh waves. Their sum is normalized to 1 at all times. The time scale has been normalized to the mean free time of the S waves in an infinite medium. (a) and (c) are predictions for the evolution of the energy for different modes for an isotropic explosion (a) at a depth $\lambda_s/3$ and for a double-couple source (c) in the x-z plane at a depth $5\lambda_s$ from the free surface. (b) and (d) are predictions for the ratio E_s/E_p of shear energy to compressional energy and the ratio H^2/V^2 of the kinetic energies associated with elastic displacements in horizontal and vertical directions. The plate thickness is $H = 20.2\lambda_s$ with $N = 106$ modes.

TABLE I. Ratio $D(\omega)/D^{\infty}(\omega)$ as a function of the number of modes $N(\omega)$ in the plate. $D^{\infty}(\omega)$ is the frequency-dependent diffusion constant for a 3D infinite medium, $D(\omega)$ is the frequency-dependent diffusion coefficient for our quasi-2D model with $N(\omega)$ modes, with the same amount of disorder in both λ and μ. Note that $D \neq D^{\infty}$ as the number of modes increases.

$N(\omega)$	3	5	13	23	43	65	85	106
$\frac{D(\omega)}{D^{\infty}(\omega)}$	0.72	0.56	0.72	0.77	0.82	0.84	0.85	0.85

It is not very difficult to show that in the equipartition regime, the generalized diffusion equation (37) further simplifies to a genuine 2D diffusion equation for the total energy density,

$$\partial_t E(\mathbf{x},t) - D(\omega)\Delta E(\mathbf{x},t) = S(\omega)\,\delta(\mathbf{x})\,\delta(t), \tag{40}$$

with diffusion constant

$$D(\omega) = \frac{\sum_{ij} D_{ij}(\omega) n_j(\omega)}{\sum_j n_j(\omega)}, \tag{41}$$

and source

$$S(\omega) = \sum_i S_i(\omega). \tag{42}$$

Equation (41) is recognized as an equipartitioned sum of all diffusion matrix elements. A similar result was obtained for the diffusion constant in an infinite elastic medium, in terms of the individual matrix elements for P and S waves [20,36,39]. Equation (40) has the simple solution,

$$E(\omega,\mathbf{x},t) = \frac{S(\omega)}{4\pi D(\omega) t} \exp\left(- \frac{\mathbf{x}^2}{4D(\omega)t} \right), \tag{43}$$

i.e., the local energy basically varies at $\mathbf{x}=\mathbf{0}$ as $E(\omega) \sim t^{-1} \times S(\omega)/D(\omega)$ at large times.

Table I shows the evolution of the ratio $D(\omega)/D^{\infty}(\omega)$ as a function of the number of modes in the plate. $D^{\infty}(\omega)$ is the elastic diffusion constant for an infinite medium, obtained by Weaver [20] and Ryzhik [23], with the same amount of disorder, i.e., as was described by Eqs. (18). The ratio varies slowly from 0.72 for $N=3$ modes to 0.85 for $N=106$, which was the thickest plate we managed to calculate within reasonable CPU time. Somewhat surprisingly, we infer that the diffusion constant does *not* seem to converge to the one of the true 3D problem. Note that our quasi-2D approximation must break down when the thickness of the plate exceeds the mean free path.

VI. COHERENT BACKSCATTERING NEAR THE FREE SURFACE

Coherent backscattering of waves is an interference effect that survives multiple scattering. It refers to a coherent enhancement of intensity near the source [39]. The effect has recently been observed with acoustic [40] and elastic waves [18,41].

We recently investigated coherent backscattering of acoustic and elastic waves [42,43]. Our analyses so far have been done either with scalar (acoustic) waves in a disordered plate with leakage [42] or with fully elastic waves in an infinite medium [43]. The last study established that the enhancement factor of coherent backscattering is highly dependent on both the nature of the source and on the precise parameter that is being measured. More specifically, a measurement of simply $\langle u_i(\omega)^2 \rangle$ of waves released by a ''double-couple'' source will hardly give rise to a coherent enhancement, so that observation is unlikely. On the other hand, the measurement of $\langle \mathrm{div}\,\mathbf{u}(\omega)^2 \rangle$ of waves released by an explosion source maps exactly onto the acoustic problem, which has the maximal enhancement factor of 2.

Both approaches are unable to model the coherent backscattering effect of wave propagation in the crust, whose elastic eigenmodes are not plane waves. In addition, an elastic measurement often takes place at the plate surface. In this section we will investigate coherent backscattering using our quasi-2D transport model. Recently, de Rosny *et al.* [18] and Weaver *et al.* [41] reported the studies of coherent backscattering of elastic waves at frequencies around 1 MHz.

Our analysis will closely follow the one given in Ref. [43]. Starting point is the calculation of the vertex $L_{nn'mm'}(\mathbf{k},\mathbf{k}',\mathbf{q})$ defined in Eq. (26) and describing the ensemble-averaged, incoherent scattering of the modes $(i,\mathbf{k}+\frac{1}{2}\mathbf{q})$ and $(i',\mathbf{k}-\frac{1}{2}\mathbf{q})$ into $(j,\mathbf{k}'+\frac{1}{2}\mathbf{q})$ and $(j',\mathbf{k}'-\frac{1}{2}\mathbf{q})$. By the reciprocity principle this object must be symmetrical with respect to left- and right-hand indices. The diffusion approximation, applied to our Q2DA model yields for large lapse times,

$$L_{ii'jj'}(\mathbf{k},\mathbf{k}',\mathbf{q}) = \frac{\delta_{ii'}\delta(\omega-\omega_{i\mathbf{k}})\,\delta_{jj'}\delta(\omega-\omega_{j\mathbf{k}'})}{-i\Omega + D\mathbf{q}^2 + \omega/Q}. \tag{44}$$

An inverse Fourier transform with respect to Ω provides the time dependence of the envelope of a wave packet with central frequency ω. Similarly, the spatial dependence is obtained by an inverse Fourier transform over $\mathbf{q}$, $\mathbf{k}$, and $\mathbf{k}'$. The result is

$$\begin{aligned} L_{ii'jj'}(\omega,t,\mathbf{x}_1,\mathbf{x}_2 \rightarrow \mathbf{x}_3,\mathbf{x}_4) &= \frac{\exp(-\omega t/Q)}{Dt}\,\delta_{ii'}\delta_{jj'} n_i n_j \\ &\times J_0(k_i \cdot x_{12}) J_0(k_j \cdot x_{34}). \end{aligned} \tag{45}$$

The depth (i.e., z) dependence can by obtained by summing over the N eigenfunctions $\mathbf{\Psi}_i \cdot (z)$ at frequency ω. The coherent backscattering is due to constructive interference of

time-reversed waves. It can be constructed straightforwardly by interchanging the indices $(i'\mathbf{x}_2)$ and $(j'\mathbf{x}_4)$ [43],

$$C_{ii'jj'}(\omega,t,\mathbf{x}_1,\mathbf{x}_2\rightarrow\mathbf{x}_3,\mathbf{x}_4) = \frac{\exp(-\omega t/Q)}{Dt}\delta_{ij'}\delta_{ji'}n_i n_j \times J_0(k_i\cdot x_{14})J_0(k_j\cdot x_{32}). \quad (46)$$

Both L and C contribute to $\langle G(i,\mathbf{x}_1\rightarrow j,\mathbf{x}_2)G^*(i',\mathbf{x}_3\rightarrow j',\mathbf{x}_4)\rangle$, but C survives only close to the source, as we shall see. To calculate actual enhancement factors, we must specify source and detector. In Eq. (28) the source was already expressed in terms of the eigenmodes $(j,\mathbf{k})$. Different sources will now be considered.

In all cases below we carry out the calculation for a plate with thickness $H=20.2\lambda_s$. This is large enough to avoid a direct influence of the boundary of the bottom surface on the coherent backscattering near the upper free surface (i.e., the interference with the mirror image of the source in the bottom plane). This calculation should thus mimic the solution for any layer that obeys $\lambda_S \ll H < \ell$. As a matter of fact, in the final profiles, the lengths H and ℓ no longer come in. We therefore *conjecture* that the obtained profiles present the solution for elastic coherent backscattering in a semi-infinite elastic random medium $(H \gg \ell)$, covered by a free surface. This is, for instance, also true for the equipartition ratios at the free surface, which were seen to be identical for a thick quasi-2D layer [17] and the semi-infinite layer [35].

A. Monopolar source at depth

We consider the source $\mathbf{f}(\mathbf{r})\sim\mathbf{f}_0(\omega)\delta^{(3)}(\mathbf{r}-\mathbf{r}_0)$, which represents a highly directional force field at position $\mathbf{r}_0$, small compared to the wavelength. Equation (28) gives $S_{j\mathbf{k}}(\omega)\sim\omega\mathbf{f}_0(\omega)\cdot\mathbf{u}_{j\mathbf{k}_j}(z_0)$ with z_0 the depth of the source. To simplify the analysis we will assume that the force is directed along the z direction. This configuration was also studied by de Rosny *et al.* [18,44] using a thin chaotic 2D silicon cavity, with only three excited Lamb waves. In addition, their detection method of heterodyne laser interferometry is only sensitive to the normal displacement $u_z(z=0)$. In seismology, the force field above may be a simple model for a volcanic eruption.

Let $\mathbf{x}$ be the horizontal distance between source and detector. The measured ''incoherent'' background is found from Eq. (45),

$$L(\mathbf{x},t)\sim\frac{\exp(-\omega t/Q)}{Dt}f_0(\omega)^2 \times\sum_i n_i|u_{i,z}(0)|^2\sum_j n_j|u_{j,z}(z_0)|^2, \quad (47)$$

which is independent of $\mathbf{x}$, but still depends on the depth z_0 of the source. The ''coherent'' contribution follows from Eq. (46),

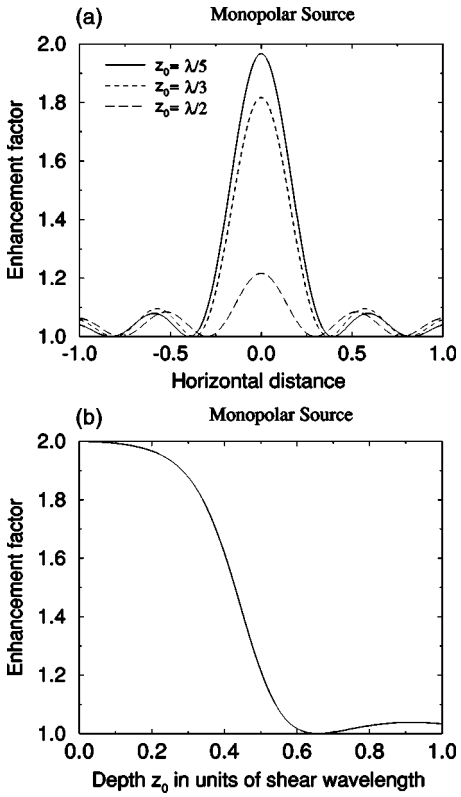

FIG. 6. Plot of the coherent backscattering enhancement for a monopolar source at a depth z_0 below the free surface, and directed along the z axis. The normal component of the displacement field $u_z(0)$ is measured at the free surface. The plate thickness $H=20.2\lambda_s$ is large enough to avoid a direct influence of the mirror image of the source in the bottom plane. This calculation should thus mimic the solution for any layer $H\gg\lambda$. (a) Plot of the backscattering cone for different depths z_0. (b) Plot of the enhancement factor at $x=0$ as a function of the source depth z_0.

$$C(\mathbf{x},t)\sim\frac{\exp(-\omega t/Q)}{Dt}f_0(\omega)^2 \times\left|\sum_i n_i u_{i,z}(0)u_{i,z}(z_0)^*J_0(k_i x)\right|^2. \quad (48)$$

As was already mentioned in previous work, the ratio $(L+C)/L$, the so-called ''enhancement factor,'' is independent of time at large lapse times [42]. An application of Cauchy's inequality shows that $(L+C)/L\leqslant 2$, with equality *if and only if* $x=0$ and if $u_{i,z}(0)=u_{i,z}(z_0)$ for all modes i. This can only be true if $z_0=0$, i.e., the source must be near the surface. In practice, to produce any measurable enhancement factor, the source must be at a depth less than the typical wavelength, as shown in Figs. 6(a) and 6(b). A source with a force direction different from normal will have a lower enhancement as well. Note that the enhancement is symmetric in azimuth around the source.

B. Isotropic explosion

An isotropic explosion at depth z_0 is described by the force field $\mathbf{f}(\mathbf{r},\omega)=B(\omega)\nabla\delta(\mathbf{r}-\mathbf{r}_0)$ [15]. It can easily be

shown that $S_{i\mathbf{k}}(\omega) = -B(\omega)\omega \operatorname{div} \mathbf{u}_{i\mathbf{k}}(\omega)$. For a fixed frequency this depends on the mode label i but, very conveniently, not on the direction $\hat{\mathbf{k}}$ of horizontal propagation.

Let us first suppose that we measure the normal component of the displacement vector at the surface. Incoherent background and coherent enhancement are given by

$$L(\mathbf{x},t) \sim \frac{\exp(-\omega t/Q)}{Dt} B(\omega)^2 \times \sum_i n_i |u_{i,z}(0)|^2 \sum_j n_j |\operatorname{div} \mathbf{u}_j(z_0)|^2,$$

$$C(\mathbf{x},t) \sim \frac{\exp(-\omega t/Q)}{Dt} B(\omega)^2 \times \left| \sum_i n_i u_{i,z}(0) \operatorname{div} \mathbf{u}_i(z_0)^* J_0(k_i \cdot x) \right|^2. \quad (49)$$

The resulting enhancement factor $(L+C)/L$ is plotted in dashed lines in Fig. 7(a) as a function of the horizontal distance, and in Fig. 7(b) for a measurement on top of an explosion source as a function of the depth z_0. Note that the enhancement never reaches its maximum value 2, not even when $z_0 = 0$. In an infinite medium, a measurement of any component of the displacement vector of waves released by an explosion source would have had no enhancement at all near the source [43]. Here, the finite enhancement is due to the nearness of a free surface.

The enhancement factor can be restored by a measurement of the dilatation $(\operatorname{div} \mathbf{u})$ in which case,

$$L(\mathbf{x},t) \sim \frac{\exp(-\omega t/Q)}{Dt} B(\omega)^2 \times \sum_i n_i |\operatorname{div} \mathbf{u}_i(0)|^2 \sum_j n_j |\operatorname{div} \mathbf{u}_j(z_0)|^2,$$

$$C(\mathbf{x},t) \sim B(\omega)^2 \frac{\exp(-\omega t/Q)}{Dt} \times \left| \sum_i n_i \operatorname{div} \mathbf{u}_i(0) \operatorname{div} \mathbf{u}_i(z_0)^* J_0(k_i \cdot x) \right|^2. \quad (50)$$

A measurement of the dilatation restores the symmetry between detector and source, and reveals the maximum enhancement factor 2 when the detector is located close to the source as shown in solid lines in Figs. 7(a) and 7(b).

C. Dipolar source

We next consider a single couple at the surface with normal displacement vector, and axis along the x axis. This source can be represented by the dipole $\mathbf{f}(\mathbf{r},\mathbf{t}) \sim \mathbf{d}(\omega)\hat{\mathbf{z}}\partial_x \delta^{(3)}(\mathbf{r}-\mathbf{r}_0)$. Such a source can be generated with laser interferometry on an elastic plate, and the resulting coherent backscattering effect was recently studied experimentally by de Rosny *et al.* [44].

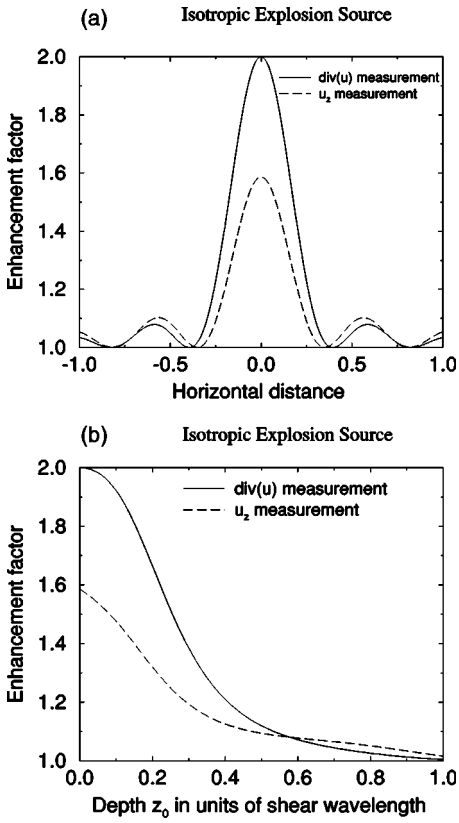

FIG. 7. Plot of the coherent backscattering enhancement for an isotropic explosion source near the free surface. Both the divergence (solid line) and the normal component of the field (dashed line) are measured. (a) Plot of the backscattering cone. (b) Plot of the enhancement factor at $x=0$ as a function of the source depth z_0. The enhancement factor only reaches its maximal value of 2 if the divergence of the field is measured and if the source is close to the surface.

The spatial derivative in the source finds its way in the Bessel functions, in the same way as was done in earlier work for the infinite system [43]. We derive, again for a measurement of the displacement vector in the direction normal to the surface,

$$L(\mathbf{x},t) \sim \frac{\exp(-\omega t/Q)}{Dt} \frac{1}{2} d(\omega)^2 \times \sum_i n_i |u_{i,z}(0)|^2 \sum_j n_j |u_{j,z}(z_0)|^2 k_j^2,$$

$$C(\mathbf{x},t) \sim \frac{\exp(-\omega t/Q)}{Dt} \cos^2\phi \, d(\omega)^2 \times \left| \sum_i n_i k_i u_{i,z}(0) u_{i,z}(z_0)^* J_1(k_i x) \right|^2. \quad (51)$$

Two things can be noted. First, C vanishes anywhere above the source ($\mathbf{x}=\mathbf{0}$). The enhancement is destroyed because the dipolar nature of the source is in some sense ''orthogonal'' to the detection of the displacement vector. Maximum enhancement actually occurs a fraction of a wavelength away from the source as shown in dashed line in Fig. 8(a). Second, the coherent enhancement around the source has a $\cos^2\phi$ struc-ture, with ϕ the azimuthal angle between the dipole axis of the source and the direction of detection. This ''double-well'' structure was observed by de Rosny, Tourin, and Fink [44].

The coherent enhancement factor can be restored by a modification of the measurement. Suppose we measure the parameter $\partial_x u_z(\mathbf{r},\mathbf{t})$. This measurement has the same symmetry as the dipolar source. We find for background and coherent enhancement,

$$L(\mathbf{x},t)\sim\frac{\exp(-\omega t/Q)}{Dt}\frac{1}{4}d(\omega)^2\sum_i n_i k_i^2|u_{i,z}(0)|^2\sum_j n_j k_j^2|u_{j,z}(0)|^2,$$

$$C(\mathbf{x},t)\sim\frac{\exp(-\omega t/Q)}{Dt}\times d(\omega)^2\left|\sum_i n_i k_i^2 u_{i,z}(0)u_{i,z}(z_0)^*\left[\frac{J_1(k_i x)}{k_i x}-J_2(k_i x)\cos^2\phi\right]\right|^2. \tag{52}$$

For $x=0$ and $z_0=0$ we infer that $L=C$, i.e., the maximal enhancement can now be reached. The plot of the restored enhancement factor as the function of the horizontal distance and as the function of the source depth are shown in solid line in Figs. 8(a) and 8(b). Note that the line profile is still not cylindrically symmetric, but depends on ϕ.

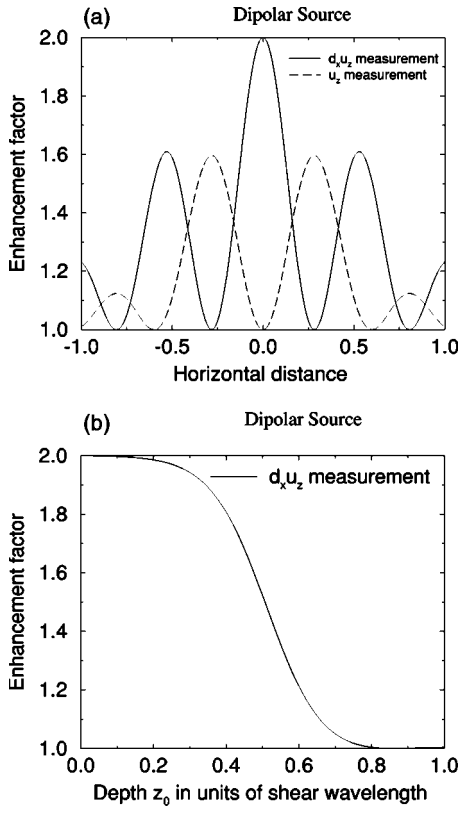

FIG. 8. Plot of the coherent backscattering enhancement for a dipolar source. Both $\partial_x u_z(\mathbf{r},\mathbf{t})$ (solid line) and the normal component $u_z(\mathbf{r},\mathbf{t})$ of the field (dashed line) are measured. (a) Plot of the backscattering cone. (b) Plot of the enhancement factor at $x=0$ as a function of the source depth z_0.

D. Double-couple source at depth

Seismic sources have successfully been modeled as two compensating couples (dipoles) [14]. To facilitate observation of coherent backscattering with seismic waves we will here obtain the enhancement expected for such a source close to a free surface. In view of the complexity of the problem, we will restrict ourselves to a seismic plane that is oriented parallel to the free surface where detection takes place. The depth of this plane is located at z_0.

The force field of a double-couple source is described by a symmetric, off-diagonal seismic tensor. We assume that the two dipoles are orthogonal and along the axes x and y. The force field is then given by

$$\mathbf{f}(\mathbf{r},\omega)=M(\omega)(\hat{\mathbf{x}}\partial_y+\hat{\mathbf{y}}\partial_x)\,\delta(\mathbf{r}-\mathbf{r}_0), \tag{53}$$

with $\mathbf{r}_0=(\mathbf{0},\mathbf{0},\mathbf{z}_0)$. We can easily check that the mode representation of the source (28) is $S_{i,\mathbf{k}}=\omega M(\omega)[k_x u_{i,y}(z_0)+k_y u_{i,x}(z_0)]$. We will assume that the measured parameter is $\partial_{y'}u_{x'}+\partial_{x'}u_{y'}$, i.e., a certain horizontal component of the stress tensor; (x',y') are the coordinates in a frame that has been rotated over an angle β with (x,y) (see Fig. 9). The displacement vector of a mode $(i\mathbf{k})$ can be expressed as

$$\mathbf{u}_{i\mathbf{k}}(\mathbf{z})=\{u_{i,z}(\mathbf{z})\hat{\mathbf{z}}+u_{i,\|}(\mathbf{z})\times[\cos\alpha_i\hat{\mathbf{k}}+\sin\alpha_i\hat{\mathbf{z}}\times\hat{\mathbf{k}}]\}\exp(i\mathbf{k}\cdot\mathbf{x}), \tag{54}$$

which introduces a new angle α_i independent of the direction $\mathbf{k}$ of propagation and of depth. Lamb waves have $\alpha_i=0$ whereas SH waves have $\alpha_i=\pi/2$. We define ϕ as the angle between $\mathbf{k}$ and the x axis, i.e., $\hat{\mathbf{k}}=\cos\phi\hat{\mathbf{x}}+\sin\phi\hat{\mathbf{y}}$. Finally, the angle μ fixes the direction of measurement $\mathbf{x}$ in the horizontal plane with respect to the source (see Fig. 9).

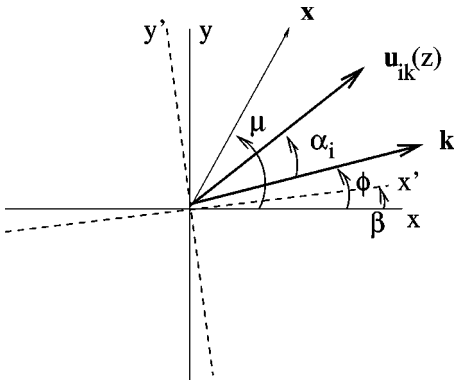

FIG. 9. The angles involved in the measurement of the backscattering cone for a dislocation source at depth z_0. See text for discussion, $\alpha_i=0$ for Lamb waves and $\alpha_i=\pi/2$ for SH waves.

The incoherent background is calculated from

$$L(\mathbf{x},t)\sim\frac{\exp(-\omega t/Q)}{Dt}M(\omega)^2\sum_i\int d^3\mathbf{k}[\partial_{x'}u_{i\mathbf{k},y'}(0)+\partial_{y'}u_{i\mathbf{k},x'}(0)]^2\mathrm{Im}\,G_{i\mathbf{k}}(\omega)\times\sum_j\int d^3\mathbf{k}'[\partial_x u_{j\mathbf{k}',y}(\mathbf{r}_0)+\partial_y u_{j\mathbf{k}',x}(\mathbf{r}_0)]^2\mathrm{Im}\,G_{j\mathbf{k}'}(\omega), \quad (55)$$

whereas the coherent enhancement follows from

$$C(\mathbf{x},t)=\frac{\exp(-\omega t/Q)}{Dt}M(\omega)^2\times\left|\sum_i\int d^3\mathbf{k}[\partial_{x'}u_{i\mathbf{k},y'}(0)+\partial_{y'}u_{i\mathbf{k},x'}(\mathbf{0})]\times[\partial_x u_{i\mathbf{k},y}(\mathbf{r}_0)+\partial_y u_{i\mathbf{k},x}(\mathbf{r}_0)]\mathrm{Im}\,G_{i\mathbf{k}}(\omega)\right|^2. \quad (56)$$

These **k** integrals can be evaluated straightforwardly and we simply quote the final result,

$$L(\mathbf{x},t)\sim\frac{\exp(-\omega t/Q)}{Dt}\frac{1}{4}M(\omega)^2\times\sum_i n_i k_i^2|u_{i,\parallel}(0)|^2\sum_j n_j k_j^2|u_{j,\parallel}(z_0)|^2. \quad (57)$$

Here, $u_\parallel$ denotes the complex amplitude of the horizontal component of the displacement vector. The coherent part is

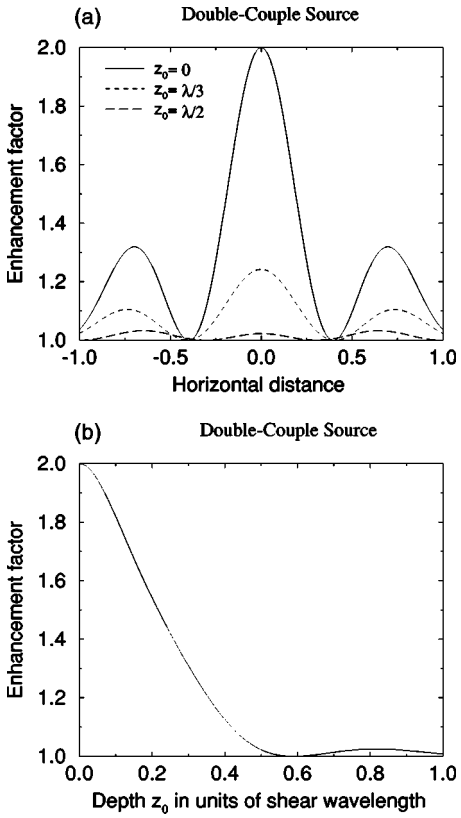

FIG. 10. Plot of the coherent backscattering enhancement for a double-couple source with both its axes along the free surface. The orientation of the detection is such that $\beta=0$ and $\mu=0$. (a) Plot of the backscattering cone for different source depths $z_0=0$, $z_0=\lambda_s/3$, and $z_0=\lambda_s/2$. (b) Plot of the enhancement factor at $x=0$ as a function of the source depth z_0.

$$C(\mathbf{x},t)\sim\frac{\exp(-\omega t/Q)}{Dt}\frac{1}{4}M(\omega)^2\times\left|\sum_i n_i k_i^2 u_{i,\parallel}(0)u_{i\parallel}(z_0)^*[\cos\beta\,J_0(k_i x)-\cos q_i J_4(k_i x)]\right|^2, \quad (58)$$

with $q_i=4\mu+3\beta$ for Lamb waves and $q_i=4\mu+3\beta+\pi$ for SH waves. Since the J_4 term is very small, the line profile is almost isotropic around $x=0$, independent of μ , and maximal for $\beta=0$. The enhancement factor $(L+C)/L$ is plotted in Fig. 10(a) as a function of the horizontal distance for different source depth and in Fig. 10(b) as a function of the source depth z_0 for a measurement on the top of the source. It is interesting to notice the relatively large second maximum of the coherent backscattering for a source at $x=0.7\lambda_s$ away from the detector ($x\approx 1.2$ km).

VII. CONCLUSIONS AND OUTLOOK

In this paper we have investigated multiple scattering of elastic modes in a two-dimensional solid plate with a thickness less than the mean free path of the waves. Contrary to

other approaches, this model facilitates an exact treatment of the boundary conditions at both sides of the plate, i.e., on the level of the elastic wave equation. At the same time, we can describe the horizontal transport of waves, as well as the intermode mixing, by a radiative transfer equation for elastic modes, which can be solved with conventional methods.

Using this equation, we have investigated different aspects, such as surface detection, mode extinction times, equipartition, polarized sources at different depths in the plate, and coherent backscattering. More concretely, we have calculated the extinction times of the different modes, and concluded that if the fluctuations of the two Lamé coefficients are comparable, many modes have a lifetime that is comparable to the *S*-wave extinction time in an infinite elastic 3D random medium. This is explained by the fact that these modes are either pure shear (SH) waves, or have an evanescent *P* component. Only the surface waves, evanescent in both *P* and *S*, and Lamb modes with an significant *P* component throughout the layer, have a longer lifetime.

We have also considered the symmetric mode-mode collision matrix that determines the dynamics of the intermodal scattering. For *N* modes it has *N* eigenvalues, among which one vanishes by energy conservation. The corresponding eigenvector represents the universal asymptotic mode occupation of any multiple scattering process with arbitrary source, with the important property of equipartition [17,33–36]. The other eigenvalues, whose order of magnitude equals the extinction rate of *S* waves in an infinite 3D random medium, determine the dynamics of the equipartition process. This depends on the initial excitations of the different modes, i.e., on nature and location of the source, and has been illustrated for explosions and ''double-couple'' sources at different depths. We have noticed that the energy released by an explosion takes a much longer time to reach equipartition.

Finally, our model facilitates the study of an important contemporary mesoscopic feature, coherent backscattering, in the presence of surface detection. This phenomenon results from the constructive interference of long wave paths in the random medium. It is well known from previous work that this phenomenon is heavily dependent on detector and source, in particular with respect to the polarization of the waves [43]. The nearby presence of a (free) surface adds an additional complexity, which can only be handled using our quasi-2D approach. The exact amount of constructive interference changes considerably as a function of source depth and source distance, and is also substantially different for different sources (force, dipole, explosion, double couple). The study presented in this paper contributes to the general understanding of coherent backscattering and might be applied to model future experiments [45,46].

One potential application of our model concerns the propagation and scattering of seismic waves in the Earth's crust in the frequency band 1–10 Hz. The mean free path ℓ of seismic waves is typically estimated to be equal to 50 to 100 km, whereas the crust depth H is around 30 km. Thus the basic criterion $\ell \gg H$ for the quasi-2D approximation to hold seems to be met. Our study could predict how fast the different guided modes mix up and finally reach equipartition. We recently observed equipartition of seismic waves and found quantitative agreement with the present model [17]. One complication is the presence of leaky modes, i.e., modes whose frequency is complex valued. The approach presented in this paper is not directly adapted to handle them, although it should apply to the guided waves in the crust. We can show that leaky waves can be included in our model [13], provided that either the leaking is weak (i.e., the leaking time is much greater than H/v), or that the leaking time is rapid compared to scattering (leaking time is much less than ℓ/v). One perspective is to understand the reported values for the decay of seismic Coda in terms of the individual quality factors of the leaky modes [47]. In future studies we will try to solve our transfer equation numerically using Monte Carlo methods.

ACKNOWLEDGMENTS

We are indebted to Michel Campillo, Ludovic Margerin, Renaud Hennino, and Celine Lacombe for many constructive discussions. This work was supported by the Groupement de Recherche ''PRIMA'' of the French CNRS and by an Action Concerté Initiative (ACI) of the French Ministry of Research.

[1] S. Chandrasekhar, *Radiative Transfer* (Dover, New York, 1960).
[2] *Wave Propagation in Complex Media*, edited by G.C. Papanicolaou (Springer-Verlag, New York, 1998).
[3] *Diffuse Waves in Complex Media*, edited by J.P. Fouque (Kluwer, Dordrecht, 1999).
[4] *Photonic Crystals and Light Localization in the 21st Century*, edited by C.M. Soukoulis (Kluwer, Dordrecht, 2001).
[5] D.S. Wiersma, A. Muzzi, M. Colocci, and R. Righini, Phys. Rev. Lett. **83**, 4321 (1999).
[6] B.A. van Tiggelen and H. Stark, Rev. Mod. Phys. **72**, 1017 (2000).
[7] M. Fink, Contemp. Phys. **37**, 95 (1996).
[8] *Waves and Imaging through Complex Media*, edited by P. Sebbah (Kluwer, Dordrecht, 2001).
[9] D.J. Thouless, J. Phys. C **5**, 77 (1972).
[10] L. Ye, G. Cody, M. Zhou, P. Sheng, and A.N. Norris, Phys. Rev. Lett. **69**, 3080 (1992).
[11] R. Dalichaouch, J.P. Armstrong, S. Schultz, P.M. Platzmann, and S.L. McCall, Nature (London) **354**, 53 (1991).
[12] A. Tourin, A. Derode, Ph. Roux, B.A. van Tiggelen, and M. Fink, Phys. Rev. Lett. **79**, 3637 (1997).
[13] C. Lacombe, M. Campillo, L. Margerin, and B.A. van Tiggelen (unpublished).
[14] K. Aki and P.G. Richards, *Quantitative Seismology: Theory and Methods* (Freeman, San Francisco, 1980).
[15] T. Lay, and T.C. Wallace, *Modern Global Seismology* (Academic Press, San Diego 1995).
[16] L. Margerin, M. Campillo, and B.A. van Tiggelen, Geophys. J. Int. **134**, 596 (1998).

[17] R. Hennino, N.P. Trégourès, N. Shapiro, L. Margerin, M. Campillo, B.A. van Tiggelen, and R.L. Weaver, Phys. Rev. Lett. **86**, 3447 (2001).
[18] J. de Rosny, A. Tourin, and M. Fink, Phys. Rev. Lett. **84**, 1693 (2000).
[19] S. Hirsekorn, J. Acoust. Soc. Am. **83**, 1231 (1987).
[20] R.L. Weaver, J. Mech. Phys. Solids **38**, 55 (1990).
[21] J. Turner and R.L. Weaver, J. Acoust. Soc. Am. **96**, 3654 (1994).
[22] J. Turner and R.L. Weaver, J. Acoust. Soc. Am. **96**, 3675 (1994).
[23] L.V. Ryzhik, G. Papanicolaou, and J.B. Keller, Wave Motion **24**, 327 (1996).
[24] G.C. Papanicolaou, L.V. Ryzhik, and J.B. Keller, Bull. Seismol. Soc. Am. **86**, 1107 (1996).
[25] P. M. Morse and H. Feshbach, *Methods of Theoretical Physics* (McGraw-Hill, New York, 1953).
[26] N. Shapiro, M. Campillo, L. Margerin, S.K. Singh, V. Kostglodov, and J. Pacheco, Bull. Seismol. Soc. Am. **90**, 655 (2000).
[27] R.L. Weaver, J. Sound Vib. **94**, 319 (1984).
[28] R.L. Weaver, internal report (unpublished).
[29] Ping Sheng, *Introduction to Wave Scattering, Localization, and Mesoscopic Phenomena* (Academic, San Diego, 1995).
[30] U. Frisch, in *Probabilistic Methods in Applied Mathematics*, edited by A. T. Barucha-Reid (Academic, New York, 1968).
[31] H. Sato and M.C. Fehler, *Seismic Wave Propagation and Scattering in the Heterogeneous Earth* (Springer-Verlag, New York, 1998).
[32] B.A. van Tiggelen and A. Lagendijk, Phys. Rep. **270**, 143 (1996).
[33] G.C. Papanicolaou, L.V. Ryzhik, and J.B. Keller, Bull. Seismol. Soc. Am. **86**, 1107 (1996).
[34] R.L. Weaver, J. Acoust. Soc. Am. **71**, 1608 (1982).
[35] R.L. Weaver, J. Acoust. Soc. Am. **78**, 131 (1985).
[36] J.A. Turner, Bull. Seismol. Soc. Am. **88**, 276 (1998).
[37] L. Margerin, B.A. van Tiggelen, and M. Campillo, Bull. Seism. Soc. Am. **91**, 624 (2001).
[38] A. Fick, Ann. Phys. (Leipzig) **170**, 59 (1855).
[39] *New Aspects of Electromagnetic and Acoustic Wave Diffusion*, edited by Research Group POAN (Springer-Verlag, Heidelberg, 1998).
[40] G. Bayer and T. Niederdränk, Phys. Rev. Lett. **70**, 3884 (1993); K. Sakai, K. Yamamoto, and K. Takagi, Phys. Rev. B **56**, 10 930 (1997).
[41] R.L. Weaver and O.I. Lobkis, Phys. Rev. Lett. **84**, 4942 (2000).
[42] L. Margerin, M. Campillo, and B. A. van Tiggelen, Geoph. J. Int. **145**, 543 (2001).
[43] B.A. van Tiggelen, L. Margerin, and M. Campillo, J. Acoust. Soc. Am. **110(3)**, 1291 (2001).
[44] J. de Rosny, Ph.D. thesis, University of Paris 6, 2000.
[45] R.L. Weaver (private communication).
[46] M. Born and E. Wolf, *Principles of Optics* (Pergamon, New York, 1975), Appendix III.
[47] L. Margerin, M. Campillo, N.M. Shapiro, and B.A. van Tiggelen, Geophys. J. Int. **138**, 343 (1999).